J|A|C|S
ARTICLES
Published on Web 01/08/2003

Chemical and Photochemical Electron Transfer of New Helianthrone Derivatives: Aspects of Their Photodynamic Activity

Shai Rahimipour,*,† Cornelia Palivan,‡ Frédérique Barbosa,‡ Itzhak Bilkis,§ Yitzhak Koch,† Lev Weiner,† Mati Fridkin,† Yehuda Mazur,† and Georg Gescheidt*,‡

Contribution from the Department of Organic Chemistry and Neurobiology, Weizmann Institute of Science, Rehovot, Israel, Department of Chemistry, University of Basel, Klingelbergstrasse 80, CH-4056 Basel, Switzerland, and Institute of Biochemistry, Food Science, and Nutrition, Faculty of Agriculture, Hebrew University, Rehovot, Israel

Received August 18, 2002; E-mail: coshai@wicc.weizmann.ac.il; georg.gescheidt@unibas.ch

Abstract: Helianthrones **2**−**4** are a new class of synthetic photosensitizers, which have a molecular skeleton related to that of hypericin. We established that irradiation of heliantrones with visible light leads to the formation of semiquinone radicals and reactive oxygen species. The structures of the paramagnetic anion species produced by electron transfer were calculated on the density functional level and investigated by cyclovoltammetry, UV/vis, and EPR/ENDOR spectroscopy. As with hypericin, the π system of the helianthrones was found to be considerably deviated from planarity, and, upon electron transfer, deprotonation in the bay region occurs. The structure of the semiquinone radicals was found to be identical in THF, DMF, and aqueous buffered solutions regardless of the means by which reduction was achieved. Semiquinone radicals can be formed via self-electron transfer between the excited state and the ground state or via electron transfer from an electron donor to the excited state of helianthrone. Therefore, the presence of an electron donor significantly enhanced the photogeneration of semiquinone and superoxide radical. The kinetic studies showed that no significant photochemical destruction of helianthrones occurred upon irradiation. Generation of superoxide and singlet oxygen upon irradiation of helianthrones was established by spin trapping techniques. This shows that both type I and type II mechanisms are of importance for the photodynamic action of these compounds.

Introduction

Perylenequinone-based molecules possess a broad range of pharmacological activities in their ground states and upon irradiation with light. One of the very well studied molecules of this type is hypericin **1** (Figure 1), a pigment isolated from St. John's wort. Hypericin is reported to act as an anticancer, antiviral, and antiretroviral agent, and to induce apoptosis.[1−4] Upon irradiation with visible light, hypericin generates singlet oxygen and superoxide ion and releases a proton to the surrounding media. Thus, hypericin can behave as an energy-, electron-, and proton-transfer agent. The photophysical properties of hypericin, such as excited-state proton transfer, singlet-oxygen sensitization, and electron transfer, are prominent topics in the literature.[5−9]

The helianthrones are structurally related to hypericin and exhibit corresponding properties. Recently, it has been shown that the helianthrones possess photodynamic activity and induce apoptosis in leukaemic cells.[10] These helianthrones are readily soluble in water and absorb light in a broad range of wavelengths, enabling them to make effective use of polychromatic light. The mechanism for the anticancer activity of helianthrones is thought to be related, at least partly, to the formation of reactive oxygen species (ROS), which are generated via electron transfer from the radical anions of the helianthrones to oxygen (type I, Scheme 1).[6,9] Helianthrone radical ions are a key intermediate in this mechanism, and their characteristics are known to reflect, to a certain extent, the characteristics of the corresponding excited state.[11,12] Hence, their geometries and electronic structures are of great interest.

† Weizmann Institute of Science.
‡ University of Basel.
§ Hebrew University.

(1) Colasanti, A.; Kisslinger, A.; Liuzzi, R.; Quarto, M.; Riccio, P.; Roberti, G.; Tramontano, D.; Villani, F. *J. Photochem. Photobiol., B* **2000**, *54*, 103−107.
(2) Meruelo, D.; Lavie, G.; Lavie, D. *Proc. Natl. Acad. Sci. U.S.A.* **1988**, *85*, 5230−5234.
(3) Prince, A. M.; Pascual, D.; Meruelo, D.; Liebes, L.; Mazur, Y.; Dubovi, E.; Mandel, M.; Lavie, G. *Photochem. Photobiol.* **2000**, *71*, 188−195.
(4) Thomas, C.; Pardini, R. S. *Photochem. Photobiol.* **1992**, *55*, 831−837.
(5) Darmanyan, A. P.; Jenks, W. S.; Eloy, D.; Jardon, P. *J. Phys. Chem. B* **1999**, *103*, 3323−3331.
(6) Hadjur, C.; Jeunet, A.; Jardon, P. *J. Photochem. Photobiol., B* **1994**, *26*, 67−74.
(7) Sureau, F.; Miskovsky, P.; Chinsky, L.; Turpin, P. Y. *J. Am. Chem. Soc.* **1996**, *118*, 9484−9487.
(8) English, D. S.; Zhang, W.; Kraus, G. A.; Petrich, J. W. *J. Am. Chem. Soc.* **1997**, *119*, 2980−2986.
(9) Weiner, L.; Mazur, Y. *J. Chem. Soc., Perkins Trans. 2* **1992**, 1439−1442.
(10) Lavie, G.; Kaplinsky, C.; Toren, A.; Aizman, I.; Meruelo, D.; Mazur, Y.; Mandel, M. *Br. J. Cancer* **1999**, *79*, 423−432.
(11) Gerson, F.; Gescheidt, G.; Häring, P.; Mazur, Y.; Freeman, D.; Spreitzer, H.; Daub, J. *J. Am. Chem. Soc.* **1995**, *117*, 11861−11866.
(12) Rahimipour, S.; Palivan, C.; Freeman, D.; Barbosa, F.; Fridkin, M.; Weiner, L.; Mazur, Y.; Gescheidt, G. *Photochem. Photobiol.* **2001**, *74*, 149−156.

10.1021/ja028189x CCC: $25.00

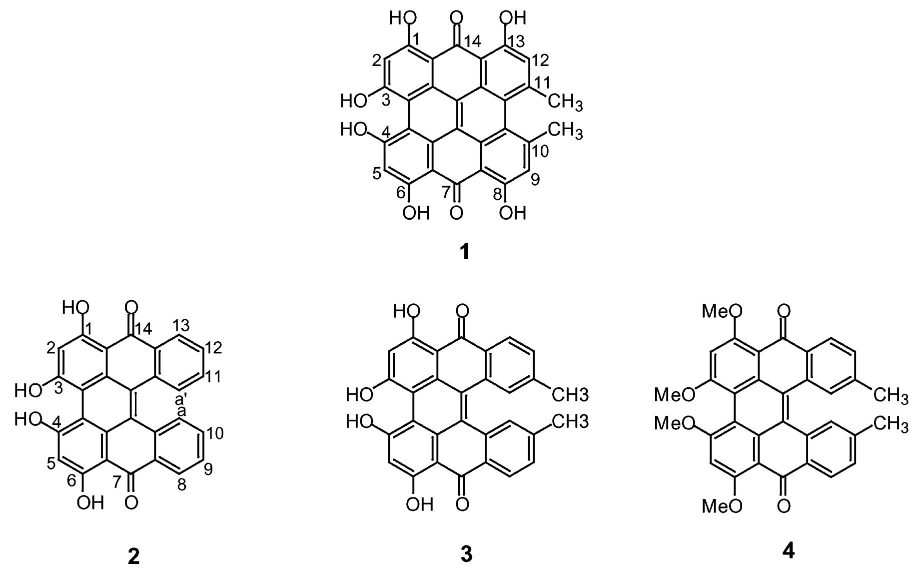

Figure 1. Structures of hypericin (**1**) and of helianthrone derivatives (**2**−**4**).

Scheme 1

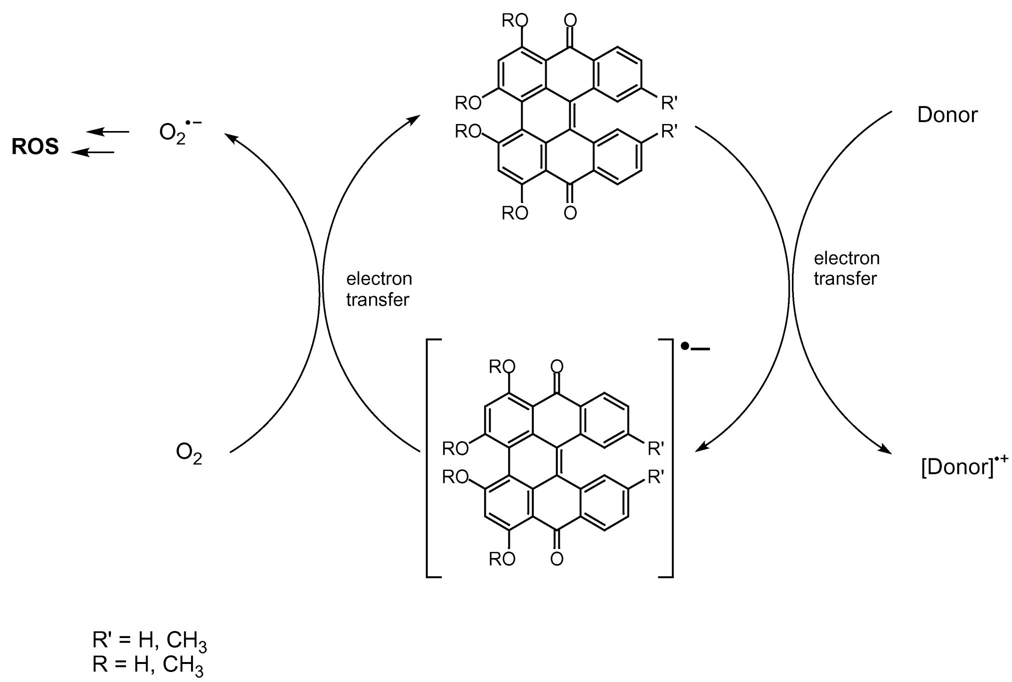

Moreover, it has also been found that liposome-bound **2** and **3** are able to generate singlet oxygen, which indicates that type II photooxidation processes can also occur. Indeed, the quantum yields of singlet oxygen from helianthrones **2** and **3** were 0.67 and 0.52, respectively, which is higher than the corresponding value of 0.35 recorded for hypericin.[13]

The subject of this contribution is to establish the structure, thermodynamic stability, and optical spectra of the radical anions of helianthrones **2**−**4** and to demonstrate their ability to form ROS. To this end, results of cyclovoltammetric measurements, quantum-mechanical calculations, EPR (ENDOR/TRIPLE), electronic spectra, and spin trapping experiments are presented.

(13) Roslaniec, M.; Weitman, H.; Freeman, D.; Mazur, Y.; Ehrenberg, B. *J. Photochem. Photobiol., B* **2000**, *57*, 149−158.

Results

Geometry of the Helianthrones. In contrast to perylenequinone, to which it is structurally related, hypericin **1** is not a planar molecule but possesses a helical shape of C_2 symmetry.[11] Geometry optimizations using ab initio 6-31G* calculations demonstrated that helianthrones **2**−**4** also have C_2 symmetry; however, due to the close vicinity of the a,a′ protons (for numbering, see Figure 1), the deviation from planarity is more pronounced than it is in hypericin **1** (Figure 2). The distance between C atoms 10 and 11 was increased from 3.1 Å in **1** to 4.6 Å in helianthrone **2**. The substitution of methyl groups at these positions in **3** and **4** does not lead to a further bending of the molecular skeleton.

Cyclovoltammetry. To determine whether the twisted geometry and the various substitution patterns at the helianthrone skeleton influence the electron-accepting and -donating proper-

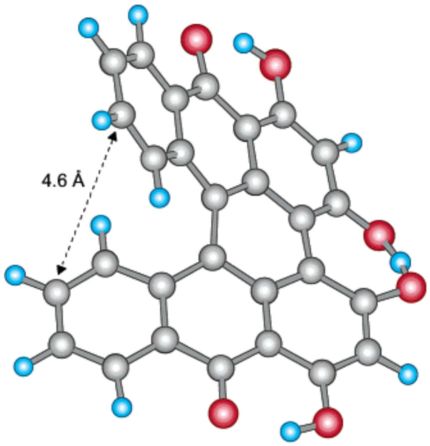

Figure 2. Geometry of deprotonated $\mathbf{2}^{2\bullet-}$ as determined by UB3LYP/6-31G* calculations.

Table 1. Redox Potentials of **1**−**4** in V vs Fc/Fc^{+}

	1 (Pt)[a]	**2** (Pt)	**3** (Pt)	**4** (Pt)	**1** (Hg)[a]	**2** (Hg)	**3** (Hg)	**4** (Hg)
$E_{1/2}^{(1)}$	−1.58	−1.43	−1.41	−1.41	−1.56	−1.43	−1.39	−1.35
$E_{1/2}^{(2)}$	−1.97	−1.75	−1.63	−1.69	−1.88	−1.74	−1.63	−1.62
$E_{1/2}^{(3)}$					−2.41	−2.23	−2.37	−2.15

[a] Values are taken from Gerson et al.[11] and are in accord with Redepenning et al.[14]

ties of these compounds, their redox potentials were determined. The cyclovoltammograms of **2**−**4** indicate rather similar features, with only modest differences being found between related redox potentials. Overall, redox potentials of the helianthrones occur at more negative voltages than does the corresponding potential for hypericin **1**. Using a platinum-disk electrode, we found that two quasi-reversible electron transfers are discernible: one at ca. −1.4 to −1.6 V versus ferrocene (Fc/Fc^{+}) and the second one at ca. −1.7 to −2.0 V versus Fc/Fc^{+}. Using a hanging mercury-drop electrode (HMDE), we found that a third redox wave at ca. −2.1 to −2.4 V versus Fc/Fc^{+} emerges for **2** and **3**, while the potentials of the first two redox processes are shifted to slightly less negative values (Table 1, Figure 3).

Similar potential shifts to less negative values were also detected when a Pt-disk electrode was replaced by a hanging mercury drop electrode for cyclovoltammetric measurements of hypericin **1**.[11] The peak-to-peak distance of the redox waves is generally close to 59 mV, indicating that no pronounced alteration of the molecular skeleton takes place.

One-Electron Reduction Reactions of 2−4 and the EPR Spectra of the Corresponding Radical Ions. Helianthrones **2**−**4** were reduced either chemically by Zn in DMF or by electrolysis employing a gold cathode. In the latter case, DMF and DMSO/PBS buffer were used as the solvents to test whether identical radicals would be formed in polar organic solvents and in aqueous solutions. Whereas helianthrones **2** and **3** gave well-defined EPR and ENDOR/TRIPLE spectra after reduction with Zn in DMF, it was not possible to obtain resolved EPR or ENDOR/TRIPLE spectra of **4** following Zn reduction. However, electrolysis of **4** in DMF generated a resolved EPR at −10 °C (not shown).

Figure 4 shows the EPR spectra of **2** and **3** upon electrolytical reduction and the corresponding ENDOR spectra after chemical reduction. The ^{1}H isotropic hyperfine coupling constants (hfcs) were detected by ENDOR/TRIPLE spectroscopy of the samples that were produced by reduction with Zn in DMF and were used for the simulation of EPR spectra (Figure 4, middle spectra). These constants were virtually identical regardless of which reduction technique and solvents were employed (Table 2). The overall widths of the EPR spectra do not exceed 10 G, which reflect the rather small ^{1}H hfcs. This suggests that the proton-bearing positions of the carbon skeleton in the radicals carry only a modest amount of spin population. Notably, simulation of **2** and **3** EPR spectra was only achievable when one ^{1}H hfc was used for two equivalent protons. The deviation between the experimental and calculated values for the protons in the 9,12 positions and the single proton attached to the oxygen atoms at C(3,4)−O is higher than that expected in view of the good to excellent agreement usually found for the UB3LYP/6-31G* calculations (Table 2).

Photochemical Reduction of 2−4 and Photogeneration of Reactive Oxygen Species. When DMF solutions of **2** and **3** were irradiated under anaerobic conditions, weak unresolved EPR spectra were observed. However, irradiation in the presence of 5% triethylamine or in alkaline aqueous solutions (KOH, pH 12) resulted in the appearance of well-resolved EPR spectra (Figure 5), which were almost identical to those obtained from electrolysis in DMF (Figure 4).

Using EPR, we also determined the kinetics of photogeneration of helianthrone semiquinones in DMF containing 5% TEA and their decay in the dark (Figure 6). The kinetic results showed a fast increase in the EPR signal, which rapidly approached plateau, followed by a slow decrease after the light was extinguished. As with hypericin, the decay of the EPR signal could be satisfactorily described as a second-order reaction.[9] Following re-irradiation of the sample, the EPR signal rose to the same amplitude reached before.

Irradiation of **2**−**4** in the presence of spin trap DMPO in aerated DMF solution resulted in the generation of 12-line EPR spectra with a characteristic hfc similar to that of the DMPO−OOH adduct (Figure 7A).[15] The presence of 5% TEA increased by about 20-fold the intensity of DMPO−OOH spin adduct (Figure 7B). Prolonged irradiation of **2** and **3** led to the disappearance of the primary EPR spectra followed by the generation of a new signal attributed to the one-electron-reduced helianthrone. Although **4** showed a reduced ability to generate the DMPO−OOH adduct as compared to **2** and **3**, the formation of DMPO−OOH in this case was not dependent on the irradiation period.

Helianthrones were also irradiated in the presence of TEMP, a well-established trap for singlet oxygen.[6] In all cases, intense 3-line EPR spectra characteristic of TEMPO ($a^{N} = 17$ G, Figure 7C) were observed. In the case of **4**, the EPR signal of TEMPO was again substantially weaker than the EPR signal observed for **2** and **3**. The presence of DABCO, a well-known singlet oxygen quencher, completely diminished the TEMPO photogeneration.[6]

SEOS Spectra. Parent helianthrones **2**−**4** exhibit several absorption bands in the range between 220 and 650 nm. Figure 8 shows the absorption bands of **3** and **4** before and after reduction. Upon reduction, an additional broad band occurred at 702 nm. The intensity of this band increased in-synch with that of the EPR signal upon prolonged contact with the Zn mirror

(14) Redepenning, J.; Tao, N. *Photochem. Photobiol.* **1993**, *58*, 532−535.
(15) Buettner, G. R. *Free Radical Biol. Med.* **1987**, *3*, 259−303.

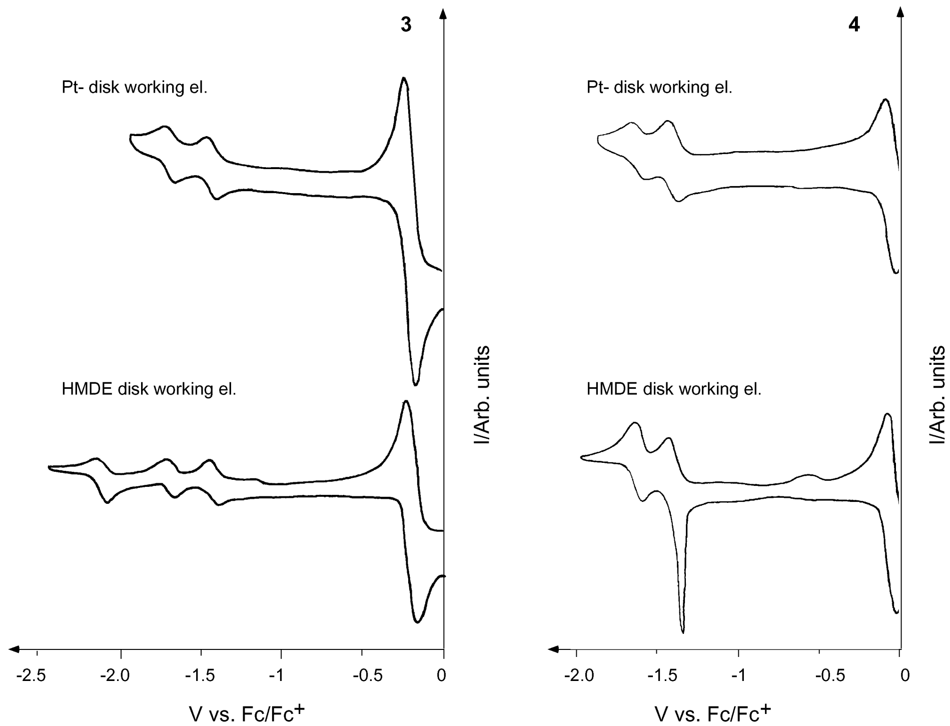

Figure 3. Cyclic voltammograms of **3** and **4** in CH_3CN recorded with a Pt disk and an HMDE working electrode using glassy carbon or platinum wire as the counter electrode. Fc/Fc^+ was used as internal standard, and *n*-Bu_4NClO_4 was used as supporting electrolyte.

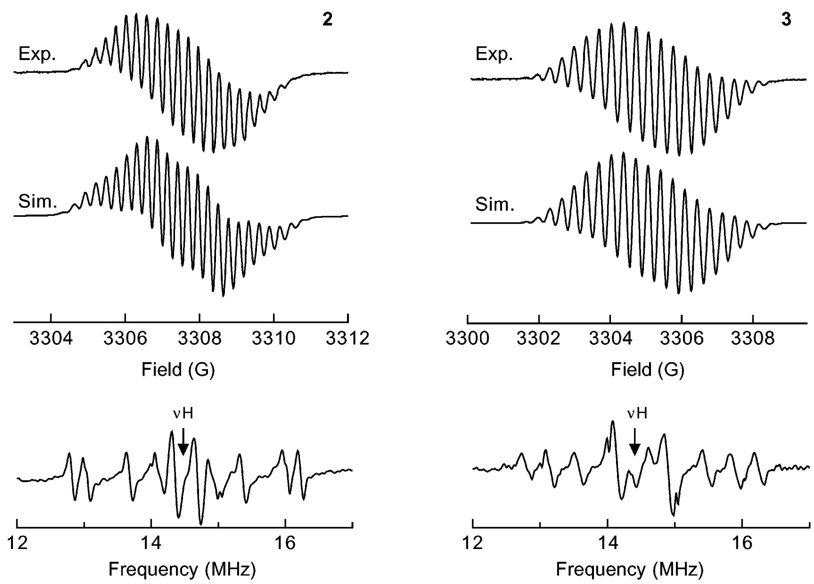

Figure 4. EPR spectra of $\mathbf{2}^{2\bullet-}$ and $\mathbf{3}^{2\bullet-}$ generated after electrolysis in 50% DMSO in PBS (pH 7.4) (top) and the corresponding ENDOR spectra (bottom) obtained after chemical reduction with Zn in DMF at −30 °C. The simulated EPR spectra (middle) were generated from the ^{1}H isotropic hfcs detected by ENDOR/TRIPLE spectroscopy of the samples produced by reduction with Zn in DMF. EPR conditions: microwave power, 5 mW; modulation amplitude, 0.02 G for **2** and 0.032 G for **3**; receiver gain, 5×10^3 for **2** and 3.2×10^3 for **3**; time constant, 1 s; scan range, 10 G; temperature, 0 °C.

(not shown). This absorption is typical for one-electron-reduced species and has been also reported upon photoreduction of hypericin in the presence of amines as electron donors.[16]

Discussion

Structure. In our previous publications on hypericin **1** and its derivatives, we showed that one acidic proton in the bay region is reduced prior to the reduction of the hypericin skeleton. This leads to the presence of an anion before one-electron reduction on the hypericin skeleton takes place. Accordingly, the first reduction stage of hypericin is not the radical anion but the radical dianion. This structure was unambiguously established by EPR spectroscopy.[11,12] In this investigation, we have used more polar solvents (DMF, DMSO/PBS) than those we used earlier (THF, 1,2-dimethoxyethane), so as to mimic physiological conditions. Therefore, the first (irreversible) redox peak of the H^+ reduction is not detectable because it is spontaneously deprotonated in the polar solvent and two (Pt

(16) Wells, T. A.; Losi, A.; Dai, R.; Scott, P.; Park, S.-M.; Golbeck, J.; Song, P.-S. *J. Phys. Chem. A* **1997**, *101*, 366−372.

Table 2. EPR Data of the Radical Ions Generated from **1**−**4** under Various Conditions and the Calculated hfcs[a]

exp. conditions	H/(OH) (8,13) 2H	H (2,5) 2H	H (a,a′) 2H	H/Me (10,11) 2/6H[b]	OH (3,4) 1H	OH (1,6) 2H	H (9,12) 2H	*g* factor
1 Zn/DMF[c]	−0.16	−0.09		1.16	1.60	−0.28	−0.91	2.0028
calc.	−0.23	−0.04		1.15	0.72	−0.60	−1.30	
2 cath./DMF	0.33	0.05	0.56	0.16	1.17	0.38	1.11	2.0005
cath./DMSO/PBS	0.28	0.08	0.53	0.27	1.33	0.33	1.10	2.0031
photolysis/DMF	0.30	0.08	0.56	0.25	1.33	0.32	1.005	
calc.	0.58	0.01	−0.93	0.08	0.80	−0.32	−1.82	
3 cath./DMSO/PBS	0.66		0.66	0.32	1.32	0.11	1.09	2.0031
photolysis/DMF	0.69		0.65	0.33	1.31	0.10	1.07	
calc.	0.63	−0.02	−0.98	0.07	0.79	−0.32	−1.86	
4 cath./DMF	0.31	0.74	0.96		0.24		1.21	2.0034
calc.	0.62	−0.94	−1.15	−0.22	0.25	−0.08	−1.62	

[a] The ^{1}H hfc (G) are taken from ENDOR spectra of Zn-reduced samples in DMF and can be utilized for the simulation of the EPR spectra taken under all applied experimental conditions (see Experimental Section). The error margin is ±5% throughout. [b] 6H for **1**, **3**, and **4** and 2H for **2**. [c] Data are obtained from Gerson et al.[11]

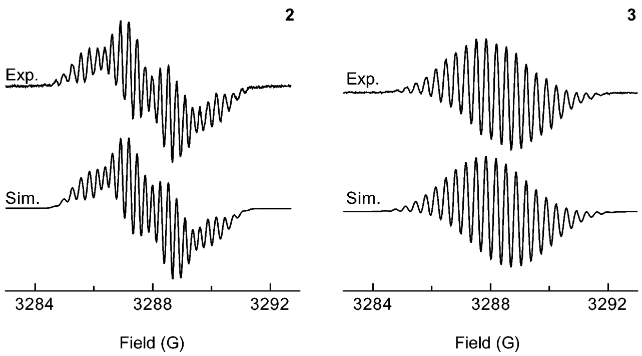

Figure 5. EPR spectra of **2** and **3** after photolysis in DMF (upper line) and the corresponding simulated spectra (lower line). DMF solutions of the helianthrones (0.1 mM) were irradiated in the presence of 5% triethylamine (helianthrone **2**) or in the presence of 5% aqueous KOH (10 mM) (helianthrone **3**). Samples were bubbled with argon for 15 min before the experiment. EPR conditions: microwave power, 0.39 mW; modulation amplitude, 0.018 G; receiver gain, 1.6 × 10^5; time constant, 0.64 s; scan range, 10 G; center of field, 3288 G; temperature, 25 °C.

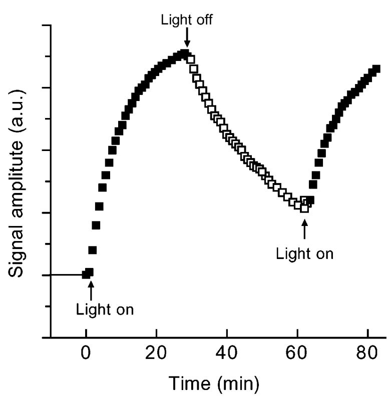

Figure 6. Dependence of the EPR signal intensity of $3^{2\bullet-}$ on irradiation time and its decay in the dark. An argon bubbled DMF solution of **3** (1 mM) containing 5% TEA was irradiated, and EPR spectra were scanned for each 45 s interval using an overmodulated condition. EPR conditions are identical to those described in the legend of Figure 5 but with a modulation amplitude of 2.5 G.

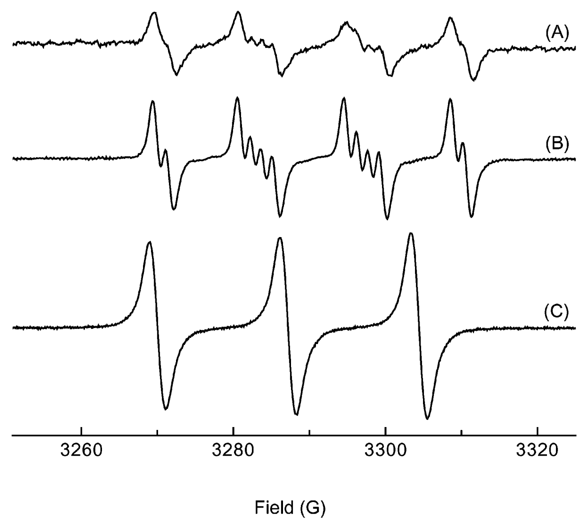

Figure 7. Photogeneration of ROS by **3** in aerated DMF. (A) The EPR spectrum of the DMPO−OOH spin adduct generated by the irradiation of **3** (0.1 mM) with DMPO (0.1 M) in DMF; (B) same as (A) but with the addition of 5% triethylamine in DMF. (C) The spectrum of TEMPO obtained from irradiation of **3** (0.1 mM) with TEMP (1 mM). EPR conditions: microwave power, 20 mW; modulation amplitude, 1.0 G; receiver gain, 4 × 10^5 for (a), 5 × 10^4 for (b), and 3.2 × 10^3 for (c); time constant, 0.64 s; scan range, 100 G; center of field, 3300 G; temperature, 25 °C.

electrode) or three (Hg electrode) quasi-reversible redox waves appear for **2**−**4** (Figure 3). These are analogous to those of **1** and its other derivatives.[12,14] Remarkably, the potentials of **2**−**4** are very similar to those established for **1** (Table 1); thus, neither methylation of the OH groups nor steric and electronic effects arising from the methyl groups substantially modify the electron-accepting properties of the helianthrones. Nevertheless, the differences between the first and second redox potentials, $|E^{(2)}_{1/2} - E^{(1)}_{1/2}|$, for the helianthrones are notably smaller than the difference found for hypericin **1**. This indicates a weaker interaction between the carbonyl groups in **2**−**4** as compared to **1** and suggests that there is a more pronounced deviation from planarity in helianthrones than in hypericin.[11]

Chemical or electrochemical reduction of **2**−**4** usually led to well-resolved EPR spectra. The EPR spectra observed upon electrolysis either in DMF or in DMSO/PBS can be readily simulated from the ^{1}H hfcs (Table 2, Figure 4). In the case of **2** and **3**, all sets of hfcs determined by ENDOR are due to two and six equivalent proton and one due to a single proton. Hfcs representing two equivalent protons arise from H and/or OH groups, such as those appearing at positions C(8) and C(13) or at positions C(1) and C(6). Hfcs representing six equivalent protons arise from the methyl substituents at positions C(10) and C(11) on helianthrone **3**. However, the single proton hfc can only be attributed to *a single H atom*. As is the case for hypericin **1**,[14] this can only occur if there is a H-bridge between C(3)−O and C(4)−O, in the bay positions of **2** and **3**. The H atom at this position has the highest hfc value (ca. 1.3 G, Table 2), and changing the number of protons for this hfc immediately

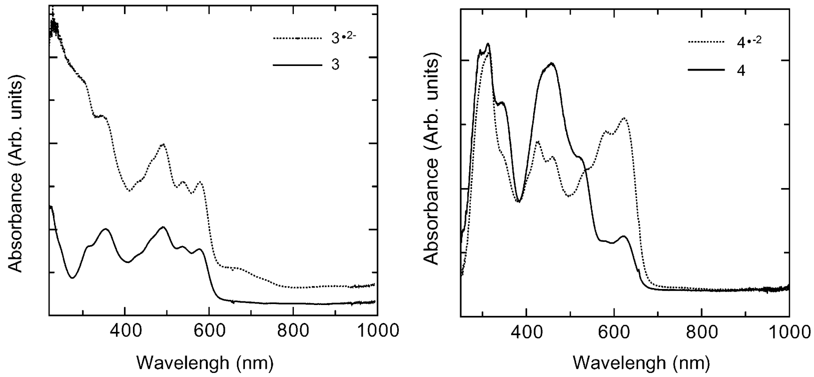

Figure 8. Optical (UV/vis) absorption spectra of **3** and **4** obtained before and after Zn reduction in DMF.

Scheme 2

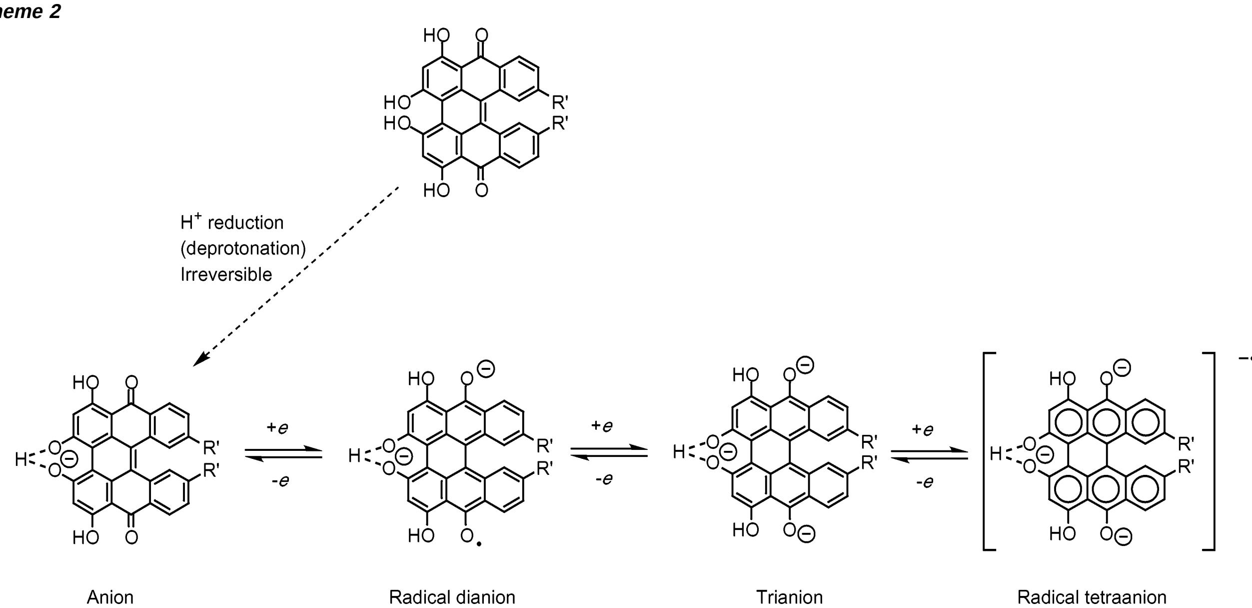

leads to a complete mismatch between the experimental and simulated EPR spectra. Thus, for **2** and **3**, one-electron reduction leads to the formation of radical dianions characterized by their EPR spectra and long-wavelength absorptions in the optical (UV/vis, SEOS) spectra (Figure 8). Further reduction leads to the trianion and radical tetraanion (Scheme 2).

It might have been expected that the replacement of the OH groups by methoxy substituents, as in **4**, and the introduction of methyl groups in the 10,11 positions, as in **3**, would have a marked influence on the electron-accepting properties and on the spin distribution in the relevant radical dianions. However, both the redox potentials (Table 1) and the ^{1}H hfcs (Table 2) of the radical ions differ only marginally from each other. The rationalization for these unexpected findings can be found in the singly occupied orbital of the radical ions. As with hypericin, helianthrone charge and spin are principally located on the central diphenoquinone moiety (Figure 8). Therefore, modification of the adjacent substituents and their deviation from planarity does not play a major role in determining electron-accepting properties and spin distribution. Moreover, substitution at positions with small orbital coefficients does not lead to a charge and spin redistribution, and even the additional negative charge at the C(3)−O and C(4)−O atoms in the bay region is too remote to attenuate the electron-accepting quality of the diphenoquinone moiety in **2**−**4**. A slight redistribution of the spin population is caused in the helianthrones, as compared to hypericin, by the different connectivity of the helianthrone π system. The missing connection between the a,a′ positions leads to ^{1}H hfc of 1.16 G for the methyl groups in the 10,11 position in **1**$^{\bullet 2-}$ being replaced by the much smaller hfc of 0.32 G in **3**$^{\bullet 2-}$. Still, the bulk of the spin and charge is confined to the biphenoquinone moiety (Figure 9).

It has been reported that hypericin **1** is present in two tautomeric conformations, the 7,14 tautomer and 1,6 tautomer.[17,18] Using quantum mechanical calculations on the density functional level of theory (UB3LYP/6-31G*), we have calculated the thermodynamic stability of both tautomers of **2**$^{\bullet 2-}$. Figure 9 shows that the spin and the charge in the two helianthrone tautomers are restricted to the biphenoquinone moiety, and, indeed, the hfcs determined for the 7,14 tautomer are not far from those calculated for the 1,6 derivative. However, according to the computed energies, the 7,14 tautomer is substantially more stable than the 1,6 tautomer ($\Delta E = 8.7$ kcal mol^{-1}). Therefore, only the calculated data of the 7,14 tautomer are used for the assignment of the experimental hfcs. Comparison of the thus obtained theoretical data with their experimental counterparts reveals a fair agreement (Table 2). No dynamic phenomena can be deduced from the temperature response of

(17) Etzlstorfer, C.; Falk, H.; Oberreiter, M. *Monatsh. Chem.* **1993**, *124*, 923−929.
(18) Mazur, Y.; Bock, H.; Lavie, D. Canadian Patent Application, 1992; Vol. 116, p 63432.

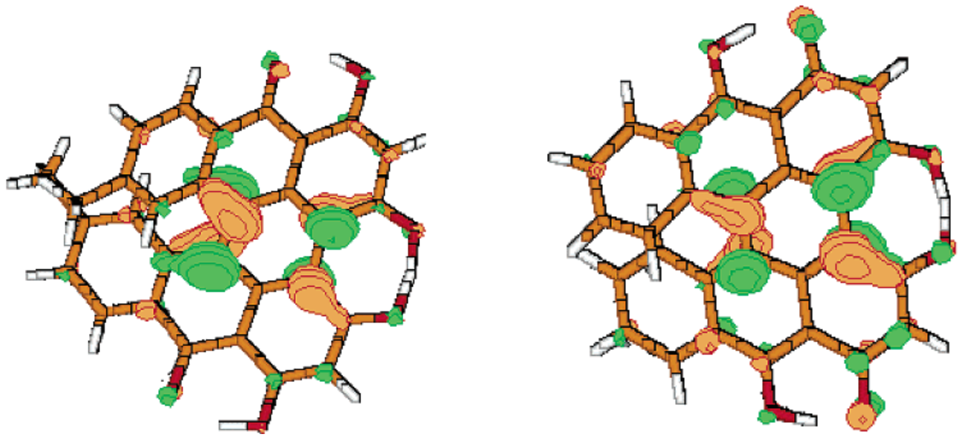

Figure 9. Comparison of the singly occupied orbitals of the 7,14 and the 1,6 tautomer of $\mathbf{2}^{2\bullet-}$.

the EPR spectra (from −25 to 25 °C). Because a fast exchange (on the EPR time scale) is likely to occur between a C(3)−OH/C(4)−O$^-$ and C(3)−O$^-$/C(4)−OH tautomer, we have calculated (using UB3LYP/6-31G*) a structure with a symmetric H-bridge between C(3)−O and C(4)−O, with the proton bound to only one of the O atoms and with the negative charge residing on the other O atom. In this case, the ^{1}H hfc of this proton increases from 0.8 to 1.4 G, which closely resembles the experimental value. The energies of the two geometries differ only by 0.6 kcal mol^{-1}; thus, the structures can be regarded as isoenergetic. Therefore, it is likely that these two tautomers interchange rapidly on the hyperfine time scale so that the overall C_2 symmetry of **2** (1,3) is not diminished to C_1 in the EPR spectra.

Photoinduced Reactivity of Helianthrones 2−4. Hypericin **1** and its derivatives are considered to be potential photosensitizers for photodynamic cancer therapy. Helianthrones, which resemble hypericin in terms of both their chemical structure and their properties, have been shown to be more phototoxic than hypericin to leukaemic cells and T-cells.[10] The cytotoxicity of these photosensitizers most likely occurs through photooxidation reactions, via two major pathways. Type I photooxidation involves a direct reaction of the excited triplet state of the sensitizer with a substrate by electron or hydrogen transfer to produce radical species other than oxygen radicals (reactions 1−3). Subsequent electron transfer from the semiquinone to molecular oxygen leads to the generation of superoxide from which hydrogen peroxide and hydroxyl radical are formed (reactions 4−6). Thus, it follows that photogeneration of helianthrone semiquinone is essential if a type I photooxidation process is to take place. In type II photooxidation, however, energy transfer occurs from the excited state of the sensitizer to the ground state of molecular oxygen ($^3O_2$) to generate singlet oxygen ($^1O_2$) as the primary oxidant (reaction 7). In contrast to type I photooxidation, type II is oxygen dependent.

The similar redox potentials of hypericin and the helianthrones suggest that helianthrones could behave as electron donors and, particularly, as electron acceptors.[9,16] Indeed, in this study we have shown that upon irradiation of helianthrones **2** and **3** in DMF, a weak unresolved EPR signal was observed. In this case, a ground-state molecule presumably donates an electron, which is accepted by an excited-state molecule (or vice versa; reaction 2; R = Sen).

$$\mathrm{Sen} + h\nu \rightarrow {}^3\mathrm{Sen}^* \tag{1}$$

$$^3\mathrm{Sen}^* + \mathrm{R} \rightarrow \mathrm{Sen}^{-\bullet} + \mathrm{R}^{+\bullet} \tag{2}$$

$$^3\mathrm{Sen}^* + \mathrm{RH} \rightarrow \mathrm{SenH}^{\bullet} + \mathrm{R}^{\bullet} \tag{3}$$

$$\mathrm{Sen}^{-\bullet} + \mathrm{O_2} \rightarrow \mathrm{Sen} + \mathrm{O_2}^{-\bullet} \tag{4}$$

$$\mathrm{O_2}^{-\bullet} + \mathrm{O_2}^{-\bullet} \xrightarrow{2\mathrm{H}^+} \mathrm{H_2O_2} + \mathrm{O_2} \tag{5}$$

$$\mathrm{H_2O_2} + \mathrm{Fe}^{2+} \rightarrow {}^{\bullet}\mathrm{OH} + {}^{-}\mathrm{OH} + \mathrm{Fe}^{3+} \tag{6}$$

$$^3\mathrm{Sen}^* + \mathrm{O_2} \rightarrow {}^1\mathrm{Sen} + {}^1\mathrm{O_2} \tag{7}$$

Adjustment of the pH to ca. 12 by addition of aqueous KOH (2.5 mM) to the DMF solution of helianthrones **2** and **3** (5:95, v:v) followed by irradiation generated an intense well-resolved EPR spectrum, which was identical to that obtained by electrolysis (Figures 4 and 5). The reported pH value for the deprotonation of the phenolic groups in hypericin and hypocrellin A is around 12.[19,20] Therefore, it is reasonable to assume that, under such basic conditions, **2** and **3** are deprotonated to their corresponding anionic forms and thus become better electron donors. Moreover, the efficient electron transfer from the anionic helianthrone to its excited state and thus the appearance of the intense EPR signal can be rationalized by assuming that helianthrones (or their anionic salt) form excimers with a sandwichlike conformation in which the quinonoid moiety overlaps with the phenolic part (phenolate). This is already known to occur with the structurally related compound, hypocrellin.[21] The formation of the anions under such conditions is consistent with a type I photooxidation mechanism. By contrast, the phenolic hydroxyl groups in **4** are blocked, and consequently no anionic species can be formed in the presence of a base, and therefore no efficient semiquinone production is possible upon irradiation. Furthermore, addition of 5% TEA generates an EPR spectrum identical to that of basic solution, which suggests that in this case TEA probably behaves as an artificial electron donor (Figure 5).[22] The second-order kinetics of the disappearance of the EPR signals after pausing the irradiation is probably related to the dismutation of the semi-

(19) Amer, A. M.; Falk, H.; Tran, H. T. N. *Monatsh. Chem.* **1998**, *129*, 1237−1244.
(20) Dumas, S.; Jardon, P.; Lepretre, J.-C.; Jeunet, A. *New J. Chem.* **2001**, *25*, 1313−1318.
(21) Diwu, Z. J.; Jiang, L. J.; Zhang, M. H. *Sci. China* **1990**, *33*, 18−26.
(22) Diwu, Z. J.; Lown, J. W. *J. Photochem. Photobiol., A: Chem.* **1992**, *69*, 191−199.

quinone to its ground-state molecule. Consequently, re-irradiation of the sample causes regeneration of the signal. This finding suggests that helianthrones do not undergo significant levels of photodestruction.

When irradiation was carried out under aerobic conditions and in the presence of DMPO as a spin trap, 12-line EPR spectra, characteristic for DMPO−OOH, were observed. The generation of the DMPO−OOH adduct reveals the efficient electron transfer from helianthrone semiquinone to molecular oxygen (reaction 4). Moreover, addition of 5% TEA as an artificial electron donor to the reaction mixture increased the intensity of the DMPO−OOH spectrum (Figure 7). This further emphasizes the involvement of helianthrone semiquinone in ROS generation and also corroborates the type I photooxidation mechanism. Prolonged irradiation of the sample caused the disappearance of the DMPO−OOH signal and the appearance of the corresponding semiquinone. Bubbling of the sample with air regenerated the DMPO−OOH signal. These results indicate that, upon irradiation, helianthrones may generate hypoxic conditions. This is an important consideration when treating malignant cells by photodynamic treatment, as hypoxic conditions can, in themselves, induce cell death.

It has been previously reported that helianthrones could also generate singlet oxygen ($^1O_2$) upon irradiation, as is known to occur with hypericin **1**.[13,23] We have evaluated the ability of helianthrones **2**−**4** to generate $^1O_2$ by employing EPR and a trapping technique. For this purpose, we have used TEMP as a spin trap for $^1O_2$. Oxidation of TEMP with $^1O_2$ generates TEMPO, which can be detected readily by its characteristic 3-line EPR spectrum.[6] Indeed, irradiation of helianthrones **2**−**4** with TEMP in aerated DMF generated the intense 3-line spectra characteristic of TEMPO (Figure 7C). The presence of DABCO as a $^1O_2$ quencher completely inhibited the appearance of the EPR spectrum of TEMPO, further confirming the presence of a type II photooxidation process. Overall, our results show that helianthrones could potentially affect cancer cells by both type I and type II photooxidation mechanisms simultaneously.

Conclusions

The present study investigated the electron-transfer behavior and the photochemical response of a new family of polycyclic quinones, helianthrones **2**−**4**, in comparison to those of hypericin. It was found that **2**−**4** are as good of electron acceptors and donors as **1** and produce a comparable electron distribution in the one-electron-reduced species. The molecular skeleton of **2**−**4** is substantially more helical (twisted) than that of **1**, which may lead to rather specific interactions with the environment.

One-electron reduction of **2** and **3**, which possess OH groups at the bay positions, in polar solvents such as DMF or DMSO/PBS, leads to the formation of radical dianions. These were characterized by EPR spectroscopy. In all cases, the same structures of the radical dianions were observed regardless of the means by which reduction was achieved. As with hypericin, the highest spin population for **2** and **3** occurs at the single hydroxyl proton at the bay region, which is consistent with the existence of an H-bridge at this position. Broad absorption bands at ca. 702 nm are characteristic for one-electron-reduced helianthrones **2** and **3**.

(23) Weiner, L.; Roth, E.; Mazur, Y.; Silman, I. *Biochemistry* **1999**, *38*, 11401−11405.

We have found that upon irradiation, these compounds effectively generate ROS, mainly superoxide radicals and singlet oxygen. These results indicate that both type I and type II photooxidation processes are occurring. Photochemical studies of **2**−**4** demonstrated that the corresponding radical ions, as established by their cyclovoltammograms and EPR spectra, act as key intermediates for the production of superoxide radical, the production of which was significantly enhanced by the presence of an electron donor. The kinetic studies showed that no significant photochemical destruction of helianthrones occurred upon irradiation. This may have a significant impact on their use in photodynamic therapy. Prolonged irradiation of **2** and **3** generates hypoxic condition, which could cause cell death. Taking into account the broad absorption range of helianthrones **2** and **4** and the presence of various electron donors in the biological system such as reduced NADH and glutathione, we regarded these compounds as promising candidates for photodynamic therapy.

Experimental Section

Unless otherwise indicated, all of the chemicals and reagents were of analytical grade. The preparation of the helianthrones is described elsewhere.[13,18] Synthesis of tetramethoxy derivatives was carried out according to published procedure.[24]

Quantum Mechanical Calculations. Quantum mechanical calculations of helianthrones were performed with the Gaussian 98 package (Gaussian Inc., Pittsburgh, PA). The geometry and the isotropic hyperfine coupling constants were calculated on the density functional level of theory (UB3LYP/6-31G*).[25−27]

EPR and ENDOR of Radicals Generated by Chemical and Electrochemical Reduction. For EPR and ENDOR experiments, the compounds were chemically reduced with zinc in *N*,*N*-dimethylformamide (DMF), which was kept over molecular sieves (Fluka, Switzerland). Electrochemical reductions were carried out employing a helical gold cathode as a working electrode and platinum wire as a counter electrode. Reductions were performed either in DMF containing 0.1 M tetra-*n*-butylammonium perchlorate (n-Bu_4NClO_4, Fluka) as the supporting electrolyte or in 30−50% phosphate buffered saline (PBS, pH 7.4) in DMSO. The supporting electrolyte was kept overnight at 100 °C prior to its use. EPR measurements were performed on a Varian-E9 instrument, while a Bruker-ESP-300 system (Bruker, Germany) was used for all ENDOR and TRIPLE-resonance studies. Simultaneous recording of the electronic absorption bands (SEOS) was performed on a J&M TIDAS-16 instrument (J&M, Germany), which was attached directly to the optical cavity of the EPR spectrometer.[28]

EPR of Radicals Generated by Photochemical Reduction and Spin Trapping Studies. For these studies, the irradiation source was a KL 1500 electronic projector lamp (Schott, Germany) employing an appropriate cutoff filter ($\lambda_{max} > 500$ nm). Samples were irradiated directly inside the EPR cavity with an optical fiber while the EPR spectra were recorded. Photochemical reduction of helianthrone was performed under anaerobic conditions by irradiating helianthrones 2−4 (0.1 mM) in DMF, or in DMF containing 5% triethylamine (v:v) or 5% aqueous KOH solution (v:v, 2.5 mM, pH ≈ 12). For kinetic studies, helianthrones (**2** and **3**, 1 mM) were irradiated in DMF containing 5% TEA. The EPR spectra were scanned every 45 s using an overmodulated condition to avoid the generation of well-resolved EPR spectra. The

(24) Agostinis, P.; Donella Deana, A.; Cuveele, J.; Vandenbogaerde, A.; Sarno, S.; Merlevede, W.; de Witte, P. *Biochem. Biophys. Res. Commun.* **1996**, *220*, 613−617.
(25) Becke, A. D. *J. Chem. Phys.* **1993**, *98*, 1372−1377.
(26) Kohn, W.; Becke, A. D.; Parr, R. G. *J. Phys. Chem.* **1996**, *100*, 12974−12980.
(27) Stephens, P. J.; Devlin, F. J.; Chabalowski, C. F.; Frisch, M. J. *J. Phys. Chem.* **1994**, *98*, 11623−11627.
(28) Gescheidt, G. *Rev. Sci. Instrum.* **1994**, *65*, 2145−2146.

accumulative kinetics were measured from the intensity of the EPR signal. For the spin trapping studies, an aerated DMF solution of either helianthrone (0.1 mM) and DMPO (0.2 M) or helianthrone and TEMP (1 mM) was irradiated in the presence or absence of 5% triethylamine (v:v) in a 200 μL EPR flat cell. To generate anaerobic conditions, argon was bubbled through the corresponding sample for 10 min prior to measurement. All spin trapping studies were performed with a Bruker electron spin resonance ER200D-SRC spectrometer at 25 °C.

Simulation of EPR Spectra. The simulations of the EPR spectra were made by using hfcs (^{1}H isotropic hyperfine coupling constants) derived from the ENDOR spectra of the samples generated from reduction with Zn in DMF and refined with the WINSIM program (NIEHS, NIH, Research Triangle Park, NC).[29]

(29) Duling, O. R. *J. Magn. Reson., Ser. B* **1994**, *104*, 105−110.

Electrochemistry. Cyclic voltammetry measurements of the tested compounds were performed on a Metrohm Polarecord E 506 and a VA scanner E 612 with a VA stand 663 (Metrohm AG, Herisau, Switzerland). All measurements were carried out at room temperature, using 0.1 M tetra-*n*-butylammonium perchlorate as the supporting electrolyte and acetonitrile as a solvent. The working electrode was either a hanging mercury drop or a platinum disk, while glassy carbon or platinum wire was used as the counter electrode. Ferrocene (Fc/Fc$^+$) was used as an internal reference ($E_{1/2}$ = 0.44 V vs Ag/AgCl).

Acknowledgment. We thank the Israel Science Foundation and the Swiss National Science Foundation for their financial support.

JA028189X